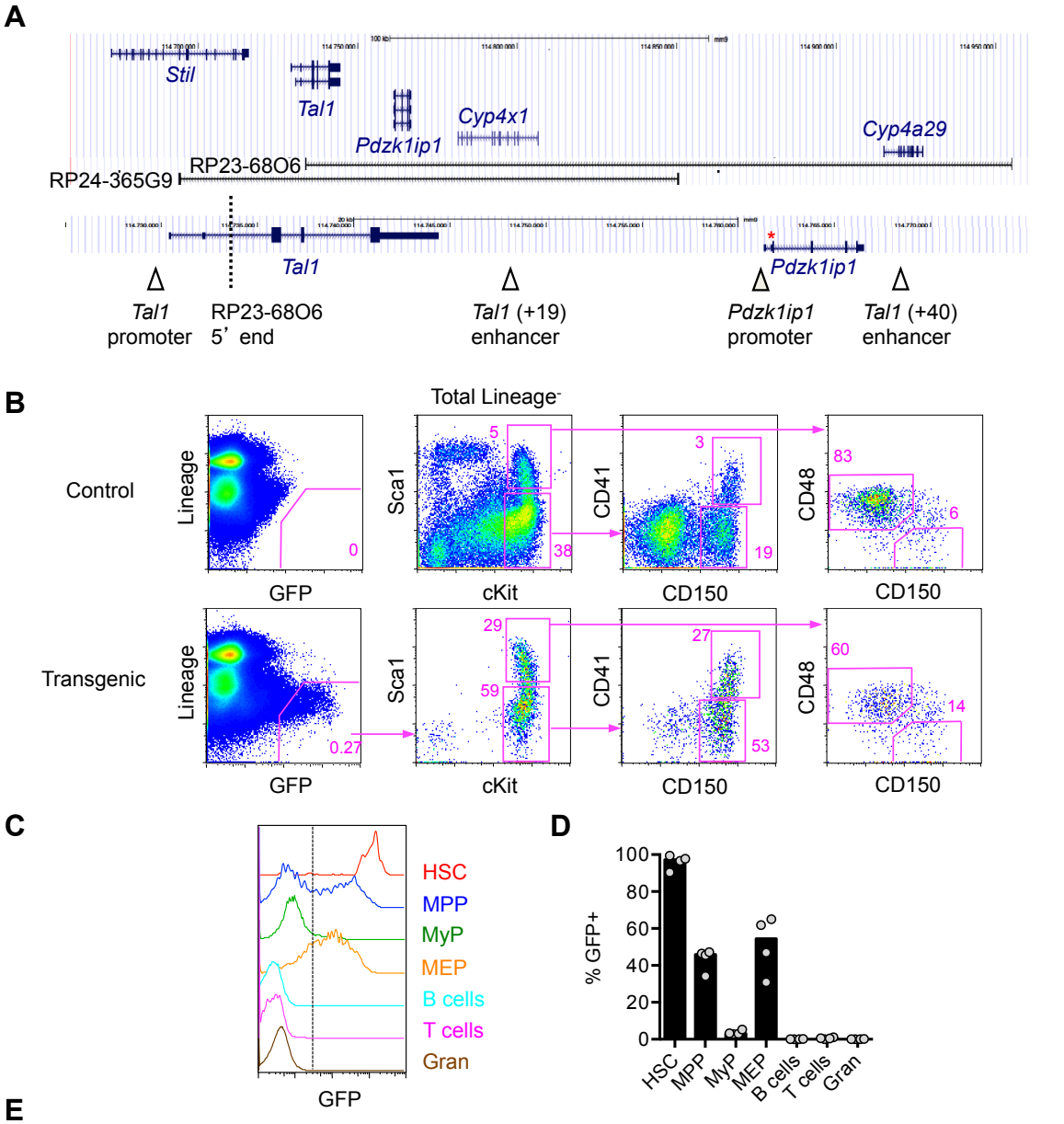

E

Phenotype						Oguro	Wilson	Pietras	Kent	Busch	this paper
CD150+	CD48-	EPCR+	CD34-/lo	Flt3-		HSC	HSC	LT-HSC	ESLAM	HSC	HSC
CD150+	CD48-	EPCR+	CD34-	Flt3-	CD229-	HSC-1					
CD150+	CD48-	EPCR+	CD34lo	Flt3-	CD229+	HSC-2	MPP1				
CD150-	CD48-	EPCRlo	CD34+ *	Flt3+ *		MPP		ST-HSC		ST-HSC	ST-HSC
CD150+	CD48+	EPCR-/lo	CD34+	Flt3-		HPC-2	MPP2	MPP2			
CD150-	CD48+	EPCR-/lo	CD34+	Flt3+		HPC-1	MPP3/4	MPP3/4		MPP	MPP

* most cells

Fig. S1 (related to Fig. 1). Expression of Pdzk1ip1 in the HSC/progenitor compartment.

A. Map of the genomic region encompassing *Pdzk1ip1* and the adjacent genes, as well as the BAC clones used to drive the transgenes (mm9 murine genome assembly visualized in the UCSC Genome Browser). The bottom panel shows the *Tal1-Pdzk1ip1* locus, indicating the regulatory regions of both genes and the 5' end of BAC RP23-68O6. The first exon of *Pdzk1ip1* used for GFP and CreER insertion is indicated by the red asterisk.

B-D. The expression of GFP reporter from the full-length *Pdzk1ip1* BAC transgene (BAC clone RP24-365G in panel A). Panel B, the expression of GFP within the BM cells of adult transgenic mice and the surface phenotype of gated GFP^+ cells; the phenotypes of total Lin^- cells are shown for comparison. Panel C, Representative histograms of GFP expression in the indicated cell populations. Panel D, the fraction of GFP^+ cells in the indicated BM cells populations (bars represent medians of values from individual animals).

E. Phenotypic definitions of HSCs and progenitor cells within the Lin^- $Sca\text{-}1^+$ $cKit^+$ (LSK) population in the adult murine BM, with representative references.

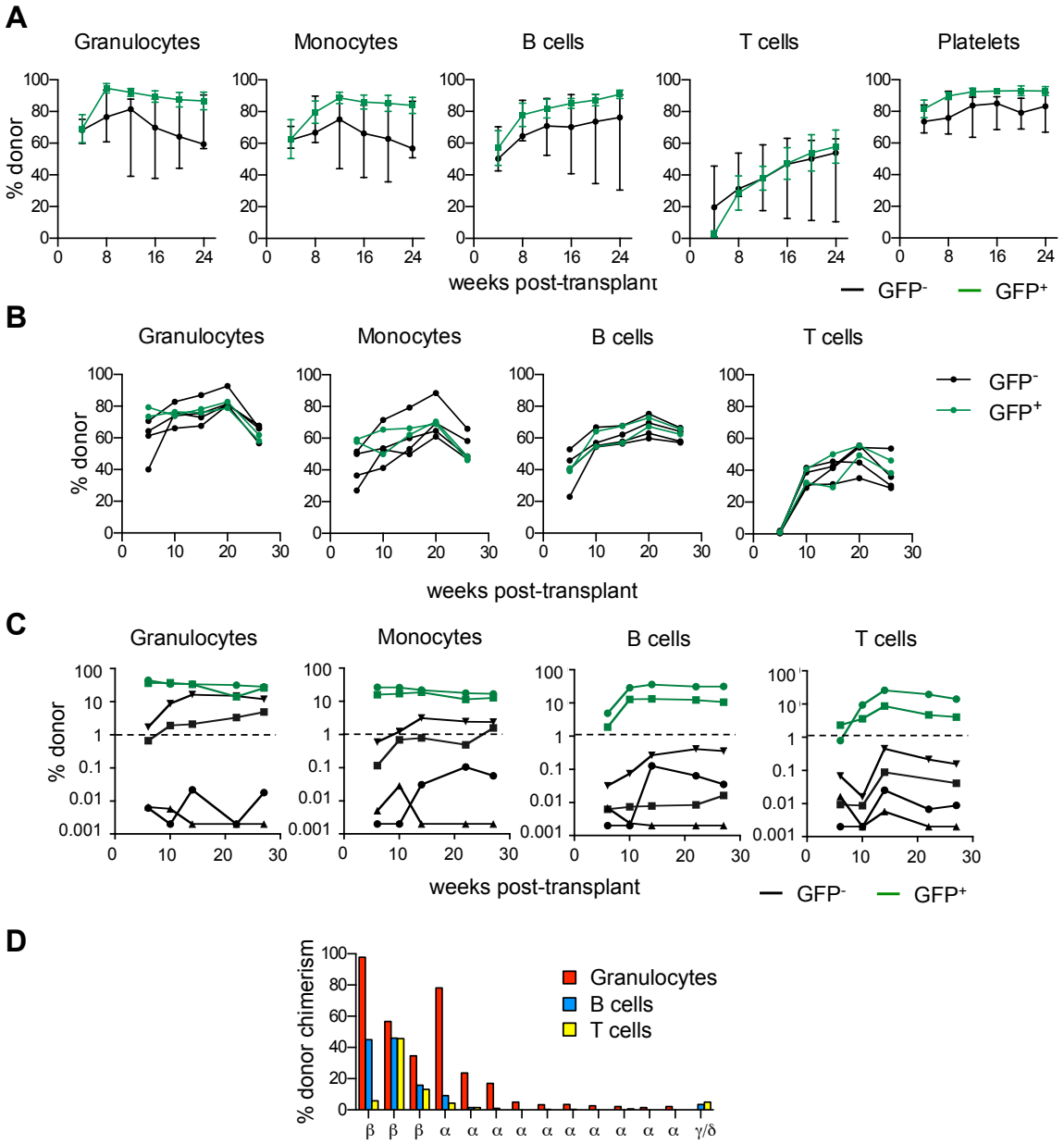

Fig. S2 (related to Fig. 2). Hematopoietic reconstitution by HSCs expressing *Pdzk1ip1*-GFP

A. Primary reconstitution of leukocytes and platelets by dsRed marked HSCs from *Pdzk1ip1*-GFP mice. GFP^+ and GFP^- LSK $CD48^-$ $CD150^+$ HSCs were sorted from the BM of *Pdzk1ip1*-GFP *Actb*-dsRed strain and transplanted (200 sorted cells/recipient) into irradiated recipient mice. Shown is the fraction of donor-derived $dsRed^+$ leukocytes and platelets in the corresponding lineages in the blood over time (median ± range of 4 animals).

B. Primary reconstitution by HSCs from *Pdzk1ip1*-GFP mice. GFP^+ and GFP^- LSK $CD135^-$ cells were sorted and transplanted in to CD45-congenic irradiated recipients (200 cells/recipient), and the proportion of donor-derived ($CD45.2^+$ $CD45.1^-$) cells among peripheral blood leukocytes was determined over time in individual recipients.

C. Secondary reconstitution by HSCs from Pdzk1ip1-GFP mice. LSK $CD135^-$ cells from the primary recipients of GFP^+ HSCs were sorted into GFP^+ and GFP^- subsets, transplanted into secondary recipients (50 GFP^+ or 200 GFP^- cells/recipient), and donor-derived mature cells were analyzed as above. Shown are data from individual recipients on the logarithmic scale; zero values were imputed for 0.002%. Dashed line indicates the 1% reconstitution threshold.

D. Hematopoietic reconstitution by single GFP^+ ESLAM HSCs. Shown are the fractions of donor-derived cells among peripheral blood granulocytes, B cells and T cells in individual recipient mice at 16 wk post-transplant (14 out of 43 total recipients). Note that a stringent reconstitution criterion (>1% donor-derived cells in any cell type) was used, resulting in a relatively low frequency of reconstituted recipients. The type of the transplanted HSCs (α, β or γ/δ) was retroactively assigned as described (Dykstra et al., 2007).

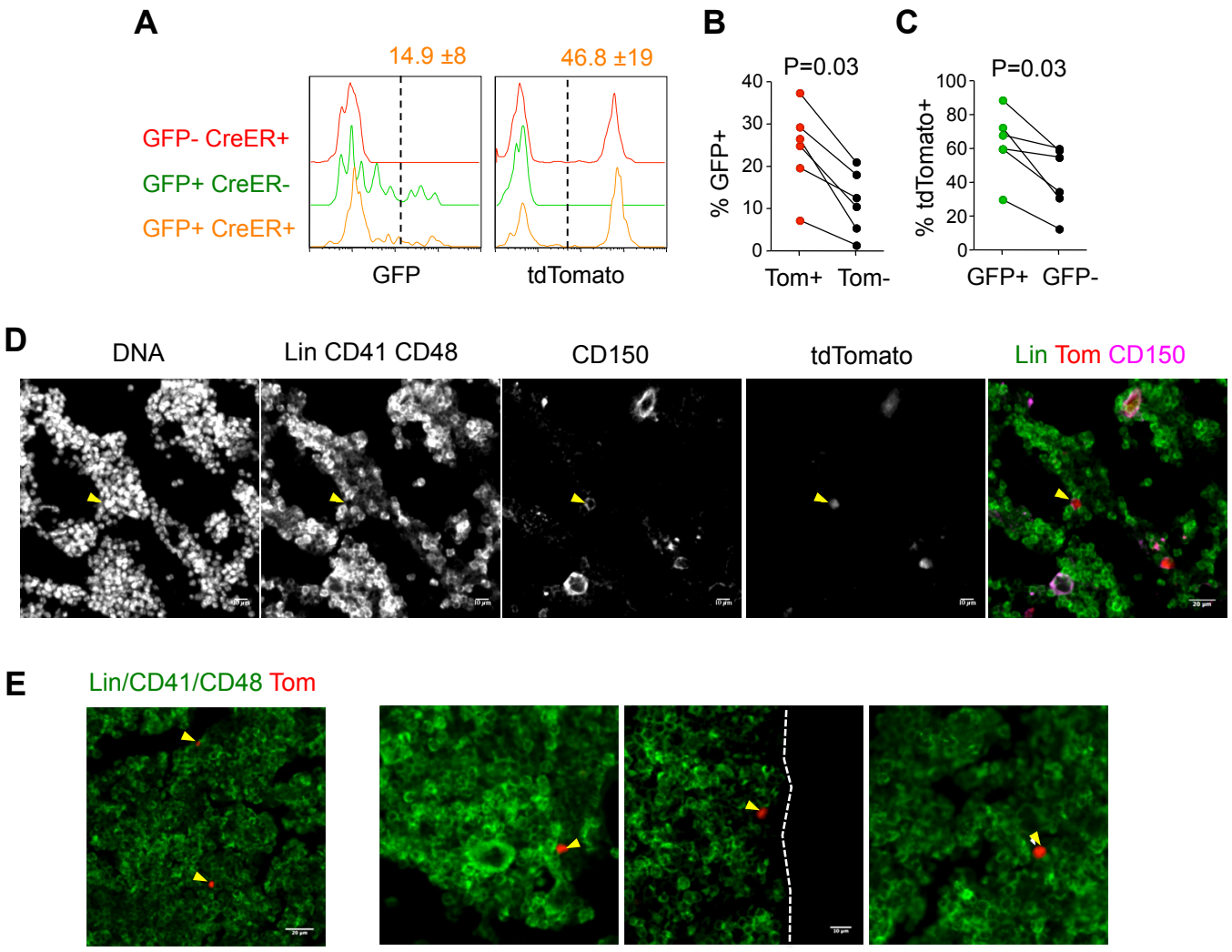

Fig. S3 (related Fig. 3). Characterization of HSCs labeled by the *Pdzk1ip1*-CreER transgene

A. The comparison of HSCs labeled by *Pdzk1ip1*-GFP and *Pdzk1ip1*-CreER transgenes. Double transgenic *Pdzk1ip1*-GFP *Pdzk1ip1*-CreER *R26*^{Tom} mice or single transgenic *Pdzk1ip1*-GFP or *Pdzk1ip1*-CreER *R26*^{Tom} controls were treated with tamoxifen to induce tdTomato (Tom) expression and analyzed 3 days later. Panel A shows representative histograms of GFP and Tom expression in the gated LSK CD48$^-$ CD150$^+$ HSCs from the single- or double-transgenic mice. The fractions of GFP$^+$ and Tom$^+$ HSCs in the double-transgenic mice are indicated above the panels (mean ± S.D. of 6 animals). Note the lower GFP labeling and higher Tom labeling compared to single-transgenic mice (Fig. 1C and 3C, respectively), likely due to interference between the transgenes. Also note that Tom expression represents a "digital" signal based on the threshold level of CreER activity, whereas GFP expression represents an "analog" signal proportional to transgene expression.

B. The fraction of GFP$^+$ cells in the Tom$^+$ versus Tom$^-$ HSCs from individual double-transgenic mice.

C. The fraction of Tom$^+$ cells in the GFP$^+$ versus the GFP$^-$ HSCs from individual double-transgenic mice.

D-E. The detection of labeled HSCs in the BM sections of *Pdzk1ip1*-CreER *R26*$^{Tom/Tom}$ mice 3 days after tamoxifen administration. Shown is immunofluorescent staining for the indicated markers and endogenous tdTomato fluorescence of non-decalcified bone sections; the Tom$^+$ HSCs are indicated (arrowheads).

D. The detection of Lin$^-$ CD41$^-$ CD48$^-$ CD150$^+$ Tom$^+$ HSCs (individual channels and merge)

E. The detection of Lin$^-$ CD41$^-$ CD48$^-$ Tom$^+$ HSCs (representative low-magnification and additional higher magnification images).

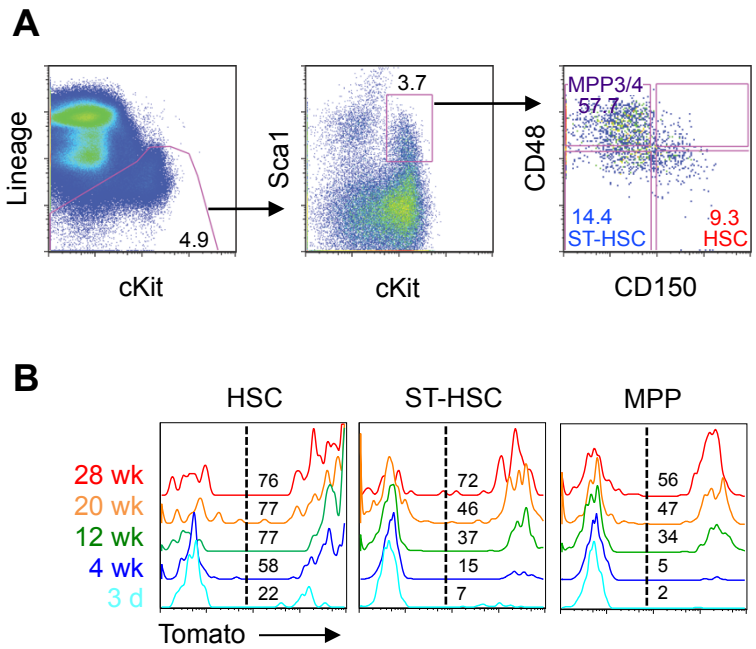

Fig. S4 (related to Fig. 4). The differentiation of labeled HSCs in *Pdzk1ip1*-CreER mice
A. The gating scheme for the definition of HSCs and their immediate progeny with the LSK population on the basis of CD48 and CD150 expression.
B. Continuous analysis of Tom^{+} cells in the HSC/progenitor compartment of tamoxifen-treated reporter mice by serial BM biopsy. Shown are histograms of Tom expression in the indicated HSC/progenitor subsets at 3 days and 4-28 weeks in a single representative animal.

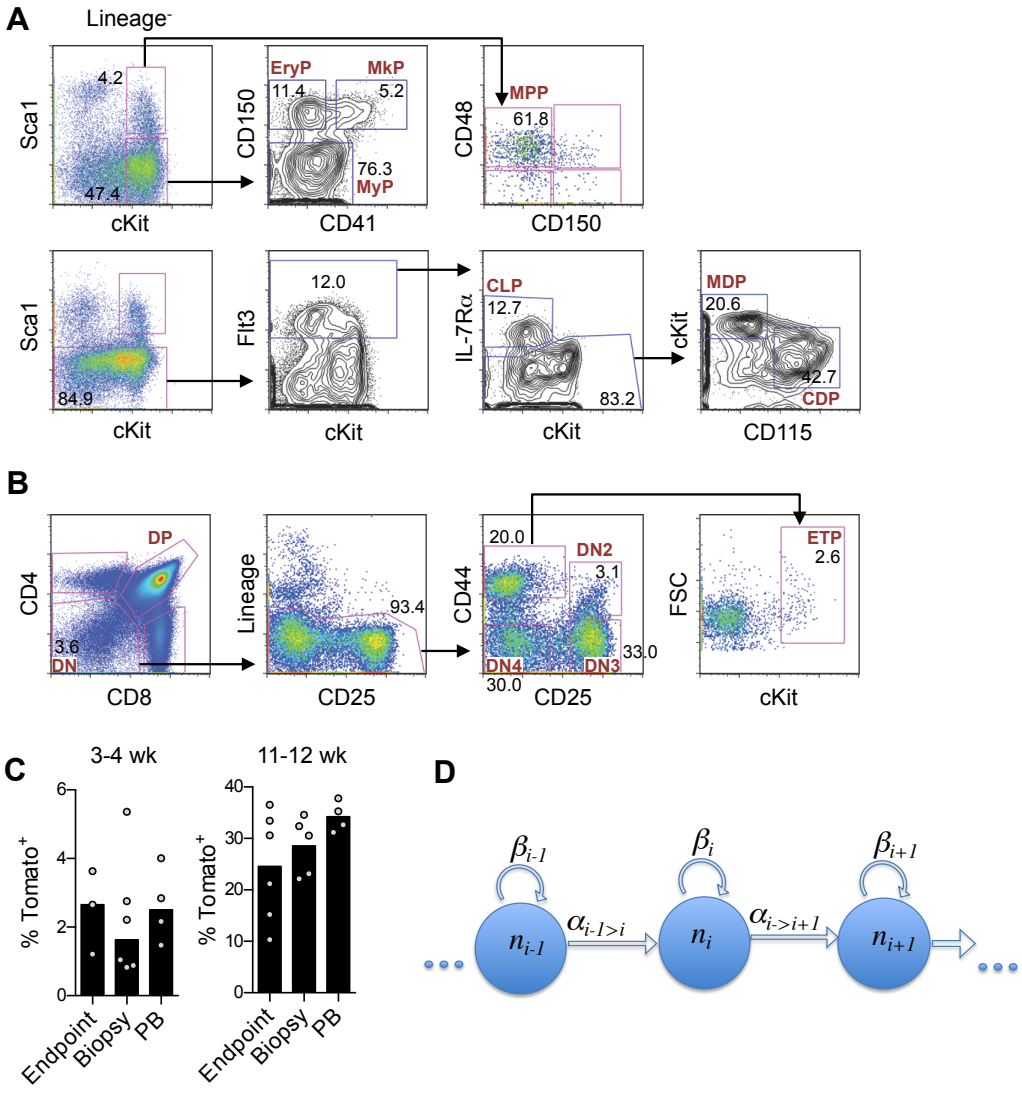

Fig. S5 (related to Fig. 5). The contribution of labeled HSCs to lineage-committed progenitors in *Pdzk1ip1*-CreER mice

A. The phenotypic definition of lineage-committed progenitors in the bone marrow, including multipotent progenitors (MPPs, Lin$^-$ Sca-1$^+$ cKit$^+$ CD150$^-$ CD48$^+$); myeloid progenitors (MyPs, Lin$^-$ Sca-1- cKit$^+$ CD150$^-$ CD41$^-$); erythroid progenitors (EryPs, Lin$^-$ Sca-1$^-$ cKit$^+$ CD150$^+$ CD41$^-$); megakaryocyte progenitors (MkPs, Lin$^-$ Sca-1$^-$ cKit$^+$ CD150$^+$ CD41$^+$); common lymphoid progenitors (CLPs, Lin$^-$ Sca-1$^-$ cKit^{lo} CD135$^+$ IL7Ra$^+$); monocyte/dendritic cell progenitors (MDPs, Lin$^-$ Sca-1$^-$ cKit^{hi} CD135$^+$ IL-7Ra$^-$); and common dendritic cell progenitors (CDPs, Lin$^-$ Sca-1$^-$ cKit^{lo} CD135$^+$ IL-7Ra$^-$ CD115$^+$).

B. The phenotypic definition of progenitors and immature T cells in the thymus, including early thymic progenitors (ETPs, Lin$^-$ CD4$^-$ CD8$^-$ CD44$^+$ CD25$^-$ cKit$^+$); double-negative thymocytes 2 (DN2, Lin$^-$ CD4$^-$ CD8$^-$ CD44$^+$ CD25$^+$), 3 (DN3, Lin$^-$ CD4$^-$ CD8$^-$ CD44$^-$ CD25$^+$) and 4 (DN4, Lin$^-$ CD4$^-$ CD8$^-$ CD44$^-$ CD25$^-$); and double-positive thymocytes (DP, CD4$^+$ CD8$^+$).

C. The effect of experimental manipulations on HSC differentiation. *Pdzk1ip1*-CreER *R26*$^{Tom/Tom}$ mice were treated with tamoxifen and either sacrificed at a single time point of 3-4 or 11-12 weeks, subjected to BM biopsy at 3 days, 4 weeks, and 12 weeks, or subjected to bleeding at 2, 4, 8 and 12 weeks. Shown is the fraction of Tom$^+$ cells among granulocytes for each treatment at 3-4 and 11-12 weeks (circles represent individual animals and bars represent median). No significant differences between treatment groups were observed at either time point.

D. The model of steady-state flows in consecutive compartments, modified from (Busch et al., 2015). Each compartment *i* is characterized by the rate of cell regeneration b_i, which equals the rate of cell division minus the rate of cell death, and the rate of differentiation into a downstream compartment $a_{i->i+1}$. Put together, these rates give the effective residence time in each compartment $t_i = 1/(a_{i->i+1}-b_i)$ that determines the label propagation kinetics. Data on label propagation were fit as described in Methods, yielding t_i for every compartment. Knowing relative sizes of each compartment n_i, we computed $a_{i->i+1}$ and b_i for each compartment.

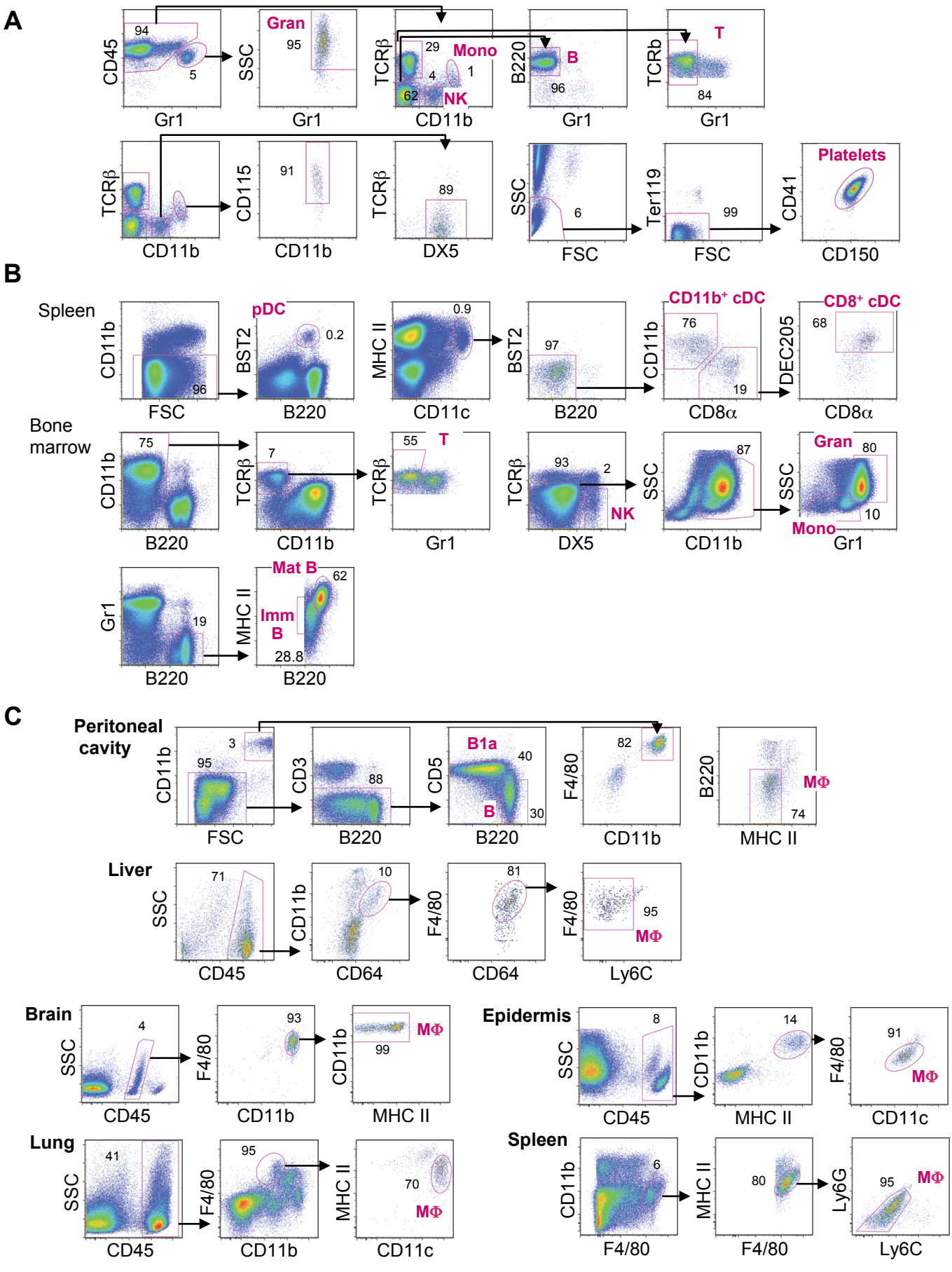
A
CD45
94
5
Gr1
SSC
Gran
95
Gr1
TCRβ
29
Mono
4
1
62
NK
CD11b
B220
B
96
Gr1
TCRb
T
84
Gr1
TCRβ
CD11b
CD115
91
CD11b
TCRβ
89
DX5
SSC
6
FSC
Ter119
99
FSC
CD41
Platelets
CD150
B
Spleen
CD11b
96
FSC
BST2
pDC
0.2
B220
MHC II
0.9
CD11c
BST2
97
B220
CD11b
CD11b⁺ cDC
76
19
CD8α
DEC205
CD8⁺ cDC
68
CD8α
Bone marrow
CD11b
75
B220
TCRβ
7
CD11b
TCRβ
55
T
Gr1
TCRβ
93
2
NK
DX5
SSC
87
CD11b
SSC
Gran
80
10
Mono
Gr1
Gr1
19
B220
MHC II
Mat B
62
Imm B
28.8
B220
C
Peritoneal cavity
CD11b
3
95
FSC
CD3
88
B220
CD5
B1a
40
B
30
B220
F4/80
82
CD11b
B220
MΦ
74
MHC II
Liver
SSC
71
CD45
CD11b
10
CD64
F4/80
81
CD64
F4/80
95
MΦ
Ly6C
Brain
SSC
4
CD45
F4/80
93
CD11b
CD11b
MΦ
99
MHC II
Lung
SSC
41
CD45
F4/80
95
CD11b
MHC II
70
MΦ
CD11c
Epidermis
SSC
8
CD45
CD11b
14
MHC II
F4/80
91
MΦ
CD11c
Spleen
CD11b
6
F4/80
MHC II
80
F4/80
Ly6G
95
MΦ
Ly6C

Fig. S6 (related to Fig. 6). The contribution of labeled HSCs to mature cells in *Pdzk1ip1*-CreER mice

A. Phenotypic definition of hematopoietic cells in the peripheral blood. Monocytes were routinely defined as $CD45^{hi}$ $CD11b^{hi}$, and were confirmed to be $CD115^{+}$. NK cells were routinely defined as $CD45^{hi}$ $CD11b^{lo}$, and were confirmed to be $DX5^{+}$. Platelets were defined by low forward and side scatter and the expression of CD41 and CD150.

B. Phenotypic definition of hematopoietic cells in lymphoid organs.

C. Phenotypic definition of hematopoietic cells in tissues. Shown are representative gating schemes for conventional ($CD5^{-}$ $B220^{+}$) and B-1a ($CD5^{+}$ $B220^{lo}$) B cells in the peritoneal cavity; macrophages (MΦ) in the peritoneal cavity (FSC^{hi} $CD11b^{+}$ $F4/80^{+}$ MHC cl II^{lo}), liver (Kupffer cells, $CD45^{+}$ $CD11b^{+}$ $F4/80^{+}$ $CD64^{+}$ Ly-$6c^{-}$), brain (microglia, $CD45^{+}$ $CD11b^{+}$ $F4/80^{+}$ MHC cl II^{lo}), epidermis (Langerhans cells, $CD45^{+}$ $CD11b^{+}$ $F4/80^{+}$ MHC cl II^{hi} $CD11c^{hi}$), lung (alveolar macrophages, $CD45^{+}$ $CD11b^{lo}$ $F4/80^{+}$ MHC cl II^{lo} $CD11c^{hi}$) and spleen ($CD11b^{lo}$ $F4/80^{+}$ MHC cl II^{lo} Ly-$6c^{-}$).

Supplemental Dataset S1 (related to Fig. 2). Differential gene expression in the HSC subsets.
The RNA-Seq data on GFP^+ and GFP^- HSC and MPP were analyzed by principal component analysis (PCA) and pairwise comparisons. “HSC vs MPP” lists genes within the main principal component, i.e. differentially expressed between both HSC populations and MPP (log_{10} change, correlation with the principal component and log_{10} values in each population). “GFP^+ vs GFP^- HSC” lists genes with >1.5-fold differential expression between the two HSC populations. Highlighted are proliferation signature genes (orange), differentiation markers (pink) and the endogenous *Pdzk1ip1* gene (green).

Supplemental Experimental Procedures

Transgenes. To generate the full-length BAC transgene, we used C57BL/6 (B6) mouse genomic BAC clone RP24-365G9 encompassing the entire *Tal1-Pdzk1ip1* locus. The clone was obtained from the Children's Hospital Oakland Research Institute (CHORI) repository and modified by recombineering in bacteria as described (Lee et al., 2001). The cassette containing enhanced green fluorescent protein (EGFP) cDNA, polyA signal and FRT-flanked bacterial zeocin resistance gene (Zeo^R) (Reizis and Leder, 2001) were recombined into the first *Pdzk1ip1* exon, and Zeo^R was removed by FLP-mediated recombination. The homology arms used for recombination were (5'->3') CAGGAGTCAAAAACACCAGCAGTGGACCGAGGTCCTACAGCTGCCTGCAGCCATG and CTAAGTCAGAGGACTGTGGCCCCGTGGTGTGTATTCACCCTCCAAAACAC. To prevent overexpression of Tal1 protein from the transgene, a Zeo^R cassette was used to replace exon 5, which encodes the Tal1 bHLH domain, and then was excised by FLP recombination. For the 5' truncated transgene, we used the B6 mouse genomic RP23-68O6 BAC clone that includes *Pdzk1ip1* but lacks the promoter and 1st exon of *Tal1*. The RP23-68O6 BAC clone with EGFP inserted into the first exon of *Pdzk1ip1* at the same position as above (generated as part of the Gene Expression Nervous System Atlas (GENSAT) Project (Gong et al., 2003)) was obtained from the CHORI repository and then used to generate the *Pdzk1ip1*-GFP strain.

To generate the *Pdzk1ip1*-CreER transgene, we introduced the fusion of Cre recombinase and optimized estrogen receptor ligand-binding domain (CreERT2) (Feil et al., 1997) into the original RP23-68O6 BAC clone (CHORI). The cassette containing CreER, polyA and Zeo^R was recombined into the first *Pdzk1ip1* exon at the same positions as EGFP, and Zeo^R was removed by FLP-mediated recombination. The recombined fragments were confirmed by sequencing, and the integrity of all BAC transgenes confirmed by conventional and pulsed-field gene electrophoresis.

BAC transgenes were digested with NotI and injected into fertilized oocytes of (B6xDBA2)F_1 hybrid mice or pure inbred B6 mice. For the *Pdzk1ip1*-GFP transgene, a founder line on outbred background generated by the GENSAT consortium was obtained from the Mutant Mouse Regional Resource Centers and used for preliminary analyses. Two additional transgenic lines were made, all showing the same expression pattern of GFP in the HSC population. The line made on the pure B6 background was then used in all subsequent experiments, and was maintained in a hemizygous state by backcrossing to pure B6 mice. To track platelet production, *Pdzk1ip1*-GFP mice were crossed with the *Actb*-dsRed mice with ubiquitous expression of dsRed (B6.Cg-Tg(CAG-DsRed*MST)1Nagy/J, Jackson Labs) (Vintersten et al., 2004).

For the *Pdzk1ip1*-CreER transgene, three founder lines were generated on the hybrid background and crossed to Cre-inducible *R26*$^{Tom/Tom}$ or *R26*$^{YFP/YFP}$ reporter strains. Two lines were found to induce reporter expression with similar specificity and efficiency, and one was chosen for all further experimentation. In pilot experiments, increasing the dose or duration of tamoxifen treatment did not increase the frequency of tdTomato expression in the HSC from the *Pdzk1ip1*-CreER *R26*$^{Tom/Tom}$ mice. The expression of tdTomato could be detected 24 hr after tamoxifen administration and reached optimal level of fluorescence by 72 hr. The latter time point was used as a start in all lineage tracing experiments.

Cell staining. Lineage marker cocktail (Lin) included Pacific blue-conjugated antibodies to B220, CD3e, CD11b, Gr1, NK1.1, and Ter119. In the *Pdzk1ip1*-GFP strain, HSC were routinely detected using the lineage cocktail and directly conjugated antibodies to CD150 (PE-Cy7); CD48 (AF647 or AF700); Sca-1 (PerCP-Cy5.5) and c-Kit (PE). In the *Pdzk1ip1*-CreER *R26*$^{Tom/Tom}$ strain, c-Kit (AF647 or APC-Cy7) and CD41 (AF488) were used.

Unless indicated otherwise, stem/progenitor types were defined as follows: HSC, Lin$^-$ Sca1$^+$ c-Kit$^+$ CD150$^+$ CD48$^-$; multipotent progenitors (MPP), Lin$^-$ Sca1$^+$ c-Kit$^+$ CD150$^-$ CD48$^+$; myeloid progenitors (MyP), Lin$^-$ Sca1$^-$ c-Kit$^+$ CD150$^-$; megakaryocyte/erythrocyte progenitors (MEP), Lin$^-$ Sca1$^-$ c-Kit$^+$ CD150$^+$. ESLAM cells were defined as follows: CD45$^+$ EPCR$^+$ CD150$^+$ CD48$^-$. Differentiated cell types were defined as follows: granulocytes, CD11b$^+$ Ly-6G$^+$ side scatter high (SSC^{hi}); monocytes, CD11b$^+$ Ly-6G$^-$ SSC^{lo}; B cells, CD11b$^-$ CD3$^-$ B220$^+$; T cells, CD11b$^-$ B220$^-$ CD3$^+$; platelets, very low forward/side scatter, CD41$^+$ CD150$^+$. Additional cell types in the BM included: immature erythrocytes, CD11b$^-$ Ter119$^+$; immature B cells, CD11b$^-$ CD45RA^{lo} MHC class II$^-$; mature B cells, CD11b$^-$ CD45RA^{hi} MHC class II$^+$.

Peritoneal cavity cells were obtained by lavage with PBS. Macrophages were isolated from mouse tissues as previously described (Greter et al., 2012; Hashimoto et al., 2013; Lavin et al., 2014). In brief, after perfusion with PBS, tissues were digested in HBSS containing collagenase type IV (Sigma) at 37°C. Brain tissue was subsequently subject to a 40% percoll-gradient centrifugation. Kupffer cells were isolated from supernatant collection, after three rounds of low speed centrifugation. Skin was digested in dispase at 37°C, epidermis and dermis were separated, and then digested in collagenase type IV.

RNA isolation, library preparation, and gene expression analysis. LSK CD48$^-$ CD150$^+$ GFP$^+$ and GFP$^-$ HSC and LSK CD48$^+$ CD150$^-$ MPP (uniformly GFP$^-$) were sorted directly into TRIzol reagent (Thermo Fisher Scientific) and RNA was extracted using the Arcturus PicoPure kit (Thermo Fisher Scientific) as described in (Lau et al., 2016). The aqueous phase of TRIzol samples was isolated, mixed with an equal volume of 70% ethanol, and then applied to PicoPure columns. Bound RNA was washed, treated with DNase I (QIAGEN) and eluted per the

manufacturer's protocol. To remove phenol contamination, the eluted RNA was resuspended in 100 ul of the PicoPure Wash Buffer 1 and loaded onto a fresh column and followed by elution.

cDNA libraries were prepared using the SMART-seq v4 Ultra Low Input RNA kit and Low Input Library Prep kit (Life Sciences) and were sequenced on an Illumina HiSeq 2500. Reads were mapped to *M.musculus* mm10 genome assembly and expression values were derived using the RNA Express software (Forster et al., 2013) implemented within the BaseSpace platform (Illumina). Clustering and pairwise comparisons were performed using the NIA Array software (Sharov et al., 2005).

Immunostaining of bone sections. Freshly isolated femurs from tamoxifen-induced *Pdzk1ip1*-CreER mice were fixed in 4% paraformaldehyde (PFA) for at 4°C, cryoprotected successively in 15% and 30% sucrose and embedded in 8% gelatin or optical cutting temperature (OCT) compound (Tissue-Tek). Longitudinal sections of 8-10 µm thickness were obtained using the CryoJane tape transfer system (Leica Biosystems) and dried overnight at room temperature. Sections were rehydrated in PBS and blocked in CAS-Block (Life Technologies) containing 20% normal goat serum. Slides were incubated with primary antibodies overnight at 4°C followed by secondary antibodies for 1 hr at room temperature with multiple washes with PBS and PBS/0.5% Triton X-100 in between. DAPI staining was applied prior to mounting with Aqua Poly/Mount (Polysciences, Inc.). Images were acquired using a Zeiss LSM 710 confocal microscope and analyzed using ImageJ software. Primary antibodies were: rat-anti-mouse CD150 (TC15-12F 12.2, Biolegend), rat-anti-mouse Endomucin (V.7C7, Santa Cruz Biotechnology), biotinylated anti-CD48 (HM48-1, Biolegend), Alexa Fluor 488-conjugated anti-CD41 (MWReg30, Biolegend), and biotinylated lineage markers (anti-Ter119, anti-B220 (6B2), anti-Gr1 (RB6-8C5), anti-CD3e (500A2), anti-CD11b (HM1/70), eBiosciences). Secondary antibodies were: Alexa Fluor 647-conjugated goat-anti-rat antibody and Alexa Fluor 488 streptavidin conjugate (Life Technologies).

Mathematical modeling. We closely followed formalism developed by (Busch et al., 2015), which was modified to take into account the dynamics of HSC compartment. Each non-HSC compartment *i* is characterized by the rate of cell regeneration b_i, which equals the rate of cell division minus the rate of cell death, and the rate of differentiation into a downstream compartment $a_{i->i+1}$. Put together these rates give the effective residence time in each compartment $t_i = 1/(a_{i->i+1}-b_i)$ that determines cellular kinetics. Population of each compartment n_i is controlled by the influx of new cells, the regeneration, and the outflow, i.e.:

$$dn_i/dt = [influx] + [population\ growth] - [outflow]$$
$$= a_{i-1->i}n_{i-1} + b_i n_i - a_{i->i+1}n_i ;$$

In steady state ($dn_i/dt = 0$) one obtains $a_{i-1->i} = (a_{i->i+1}-b_i)\ n_i/n_{i-1} = n_i/(t_i n_{i-1})$ allowing to compute upstream differentiation rate from estimated t_i and measured relative compartment sizes. Kinetics of labeled cells (n^*_i) propagation is driven by the same equation: $dn^*_i/dt = a_{i-1->i}n^*_{i-1} + b_i n^*_i - a_{i->i+1}n^*_i = a_{i-1->i}n^*_{i-1} + n^*_i/t_i$. Dividing by n_i and using steady state condition $a_{i-1->i}/n_i = 1/(t_i n_{i-1})$ from above, Busch et al. obtained an expression for the fraction of labeled cells $f_i = n^*_i/n_i$

$$df_i/dt = (f_{i-1}-f_i)/t_i ,$$

which can be fit to the data to obtain the values of t_i for each compartment. The formalism can be generalized to branching processes by using the sum of two outflows for each branching point.

Data fitting and parameter estimation: The values of t_i were estimated by non-linear optimization of the mean square difference between data and model *f(t)* computed using initial conditions $f_i(t=0) = f_{0,i}$ which determines initial fraction of labeled cells in each compartment. Additionally, and deviating from Busch et al., HSC was modeled as a compartment with initial labeled fraction $f_{HSC}(t=0)=f_{0,HSC}$ and the maximal labeled fraction $f(t=+inf)=f_{max}$:

$$f_{HSC}(t) = f_{max} - (f_{max} - f_0)\exp(-t/t_{HSC})).$$

The values of t_i and $f_{0,i}$ were fit simultaneously for all compartments and all time points. We obtained similar results from a two-stage fitting procedure: at the first stage we used HSC kinetics to estimate t_{HSC}, f_{max}, f_0 and fixed these parameters; at the second stage, we fit data for all other compartments estimating t_i and $f_{0,i}$, conditioning on $f_{0,i} < f_0$. The fits were done individually for each mouse.

Kinetics of HSC compartment: We assume that HSC compartment includes two populations of cells: "top-level" HSC (HSC0) and their progeny (HSC1). Here we show how fitting parameters for HSC compartment allows to estimate parameters of HSC0 and HSC1.

If $w = n_{HSC1}/(n_{HSC1} + n_{HSC0})$ is the fraction of the progeny cell, then the fraction of labeled cells is the HSC compartment is

$$f_{HSC} = (1-w)f_{HSC0} + w\ f_{HSC1} = (1-w)f_{HSC0} + w\ f_{HSC1}$$

Since top-level HSCs are fully self-renewing f_{HSC0} should be constant, and all labeling kinetics in the HSC compartment is due to HSC1, i.e. $t_{HSC1} = t_{HSC}$ that is estimated from the data. If the fraction of initially labeled top-level HSC is a_0 (i.e. $f_{HSC0}(t) = a_0 = const$) and the progeny was initially unlabeled, then

$$f_{HSC}(t) = (1-w)\ a_0 + w(1-exp(-t/t_{HSC})).$$

Since $f_{HSC}(t)$ is fit as $f_{HSC}(t) = f_{max} - (f_{max} - f_0)\exp(-t/t_{HSC}))$, *w* and *a* are obtained as

$$w = 1 - f_0/f_{max};\ a_0 = (f_{max} - f_0)/w;$$

If we assume that a small fraction a_1 of the progeny has been initially labeled as set its value to as little as in the downstream compartments (<10%), then *w* can be found as a solution of quadratic equation $a_1 w^2 - f_{max} w + f_{max} - f_0 = 0.$

This approach allows to estimate parameters of HSC0 and HSC1. Moreover, this approach provides the value of $n_{HSC0}/n_{HSC1}=(1-w)/w$ that together with t_{HSC} gives an estimate of the rate of top-level HSC differentiation $a_{HSC0->HSC1} = n_{HSC1}/(n_{HSC0}\ t_{HSC})$, which also suppose to equal b_{HSC0} for a self-renewing compartment. Rates of regeneration for HSC1 cells are estimated as for all other compartments using $n_{HSC1}=w\ n_{HSC}$. In summary, parameters of top-level HSC and their progeny cells can be estimated from measurements for the aggregated HSC compartment.

Supplemental References

Busch, K., Klapproth, K., Barile, M., Flossdorf, M., Holland-Letz, T., Schlenner, S.M., Reth, M., Hofer, T., and Rodewald, H.R. (2015). Fundamental properties of unperturbed haematopoiesis from stem cells in vivo. Nature *518*, 542-546.

Dykstra, B., Kent, D., Bowie, M., McCaffrey, L., Hamilton, M., Lyons, K., Lee, S.J., Brinkman, R., and Eaves, C. (2007). Long-term propagation of distinct hematopoietic differentiation programs in vivo. Cell Stem Cell *1*, 218-229.

Feil, R., Wagner, J., Metzger, D., and Chambon, P. (1997). Regulation of Cre recombinase activity by mutated estrogen receptor ligand-binding domains. Biochem Biophys Res Commun *237*, 752-757.

Forster, S.C., Finkel, A.M., Gould, J.A., and Hertzog, P.J. (2013). RNA-eXpress annotates novel transcript features in RNA-seq data. Bioinformatics *29*, 810-812.

Gong, S., Zheng, C., Doughty, M.L., Losos, K., Didkovsky, N., Schambra, U.B., Nowak, N.J., Joyner, A., Leblanc, G., Hatten, M.E.*, et al.* (2003). A gene expression atlas of the central nervous system based on bacterial artificial chromosomes. Nature *425*, 917-925.

Greter, M., Helft, J., Chow, A., Hashimoto, D., Mortha, A., Agudo-Cantero, J., Bogunovic, M., Gautier, E.L., Miller, J., Leboeuf, M.*, et al.* (2012). GM-CSF controls nonlymphoid tissue dendritic cell homeostasis but is dispensable for the differentiation of inflammatory dendritic cells. Immunity *36*, 1031-1046.

Hashimoto, D., Chow, A., Noizat, C., Teo, P., Beasley, M.B., Leboeuf, M., Becker, C.D., See, P., Price, J., Lucas, D.*, et al.* (2013). Tissue-resident macrophages self-maintain locally throughout adult life with minimal contribution from circulating monocytes. Immunity *38*, 792-804.

Lau, C.M., Nish, S.A., Yogev, N., Waisman, A., Reiner, S.L., and Reizis, B. (2016). Leukemia-associated activating mutation of Flt3 expands dendritic cells and alters T cell responses. J Exp Med.

Lavin, Y., Winter, D., Blecher-Gonen, R., David, E., Keren-Shaul, H., Merad, M., Jung, S., and Amit, I. (2014). Tissue-resident macrophage enhancer landscapes are shaped by the local microenvironment. Cell *159*, 1312-1326.

Lee, E.C., Yu, D., Martinez de Velasco, J., Tessarollo, L., Swing, D.A., Court, D.L., Jenkins, N.A., and Copeland, N.G. (2001). A highly efficient Escherichia coli-based chromosome engineering system adapted for recombinogenic targeting and subcloning of BAC DNA. Genomics *73*, 56-65.

Reizis, B., and Leder, P. (2001). The upstream enhancer is necessary and sufficient for the expression of the pre-T cell receptor alpha gene in immature T lymphocytes. J Exp Med *194*, 979-990.

Sharov, A.A., Dudekula, D.B., and Ko, M.S. (2005). A web-based tool for principal component and significance analysis of microarray data. Bioinformatics *21*, 2548-2549.

Vintersten, K., Monetti, C., Gertsenstein, M., Zhang, P., Laszlo, L., Biechele, S., and Nagy, A. (2004). Mouse in red: red fluorescent protein expression in mouse ES cells, embryos, and adult animals. Genesis *40*, 241-246.